

Award Accounts

The Chemical Society of Japan Award for Young Chemists for 2003

Dynamical Interactions between Solute and Solvent Studied by Three-Pulse Photon Echo Method

Kaoru Ohta* and Keisuke Tominaga*,[1]

Graduate School of Science and Technology, Kobe University, Nada-ku, Kobe 657-8501

[1]Molecular Photoscience Research Center, CREST/JST, Kobe University, Nada-ku, Kobe 657-8501

Received January 5, 2005; E-mail: kohta@kobe-u.ac.jp

This account summarizes our recent work on measurements of the correlation function of the transition frequency fluctuations by a three-pulse photon echo method. The correlation function of the transition frequency fluctuations is a sensitive measure for the magnitudes and time scales of dynamical interactions between solute and solvent. We describe the results of the solvation dynamics of small ions in protic solvents such as methanol and water obtained by an infrared photon echo method.

As is well known, the interactions between solute and solvent play an important role in chemical reaction dynamics and in many relaxation processes in the condensed phase.[1–3] In liquids, the positions and the directions of the solvent molecules are fluctuating in time due to the thermal motions. Solvent fluctuation is a characteristic feature of a liquid that is not seen in the gas and solid phase. Solute–solvent interactions induce energy exchange between the solute and the solvent, and the competition between the intramolecular and intermolecular energy relaxation affects the chemical reaction dynamics.[1–3] Therefore, it is important to know not only the time scales of solvent fluctuation but also the magnitudes of the solute–solvent interactions to characterize the dynamical interaction between solute and solvent.[4,5]

One of the traditional ways to obtain information on dynamical fluctuations of the solvent molecules and on the magnitudes of the solute–solvent interaction is to analyze the lineshapes of the absorption spectrum of the solute molecule.[6] In contrast to the gas phase, the linewidth of the absorption spectrum in solution is always broadened and featureless. Due to the modulation of the energy difference between the ground and excited states by the solute–solvent interaction, the electronic or vibrational transition frequency of the solute molecule fluctuates in time to induce a broadening of the spectrum. Therefore, lineshapes contain rich information on the dynamical interaction with the environment.[7] Generally, the spectral broadening has been classified into two limiting cases; i.e., homogeneous and inhomogeneous broadening. In the homogeneous broadening limit, the fluctuation of the transition frequency is very fast compared to the observation time window.[8] In the inhomogeneous broadening limit, each solute molecule possesses a different transition frequency due to the heterogeneity of the local structure in solution. In this case, the fluctuation of the transition frequency is very slow compared to the observation time window.[8] However, we always have a certain ambiguity in separating the two contributions to the lineshape. In particular, the electronic absorption or fluorescence spectrum is complicated due to the presence of the vibronic structures. It is always difficult to obtain valuable information on dynamical interaction with the surrounding solvents just based on the lineshape of the electronic absorption and/or fluorescence spectra since the congestion of many vibronic transitions obscures the underlying solvent dynamics.

Over more than twenty years, ultrafast spectroscopy has become a powerful and popular tool to investigate various dynamical processes in real time.[1–3,9] These techniques have been applied to study the chemical reaction dynamics and many relaxation processes of the solute and solvent molecules in solution. Various methods including dynamic fluorescence Stokes shift measurement and photon echo spectroscopy have been developed to study the dynamical interaction between solute and solvents, i.e., solvation dynamics.[10–17] In parallel, significant progress in many theoretical methods has been made in an attempt to gain a more detailed molecular mechanism of the solute–solvent interactions.[18] Among various experimental methods, a dynamic fluorescence Stokes shift measurement is one of the most popular ones to investigate the solvation dynamics in the electronically excited state.[10] In this experiment, one can monitor the response of the solvent molecules after a sudden change of the charge redistribution of the solute molecule due to photoexcitation. Dynamic fluorescence Stokes shift is a sensitive probe for the solvation process where the configuration of the solvent molecules relaxes to a more energetically favorable situation. In a certain limit, the time dependence of the dynamic Stokes shift function is identical to the correlation function of the transition frequency fluctua-

Published on the web August 30, 2005; DOI 10.1246/bcsj.78.1581

tions which we will discuss in detail later.[4] Therefore, the observed dynamics in the dynamic fluorescence Stokes shift measurement is connected very closely with the dynamical fluctuations of the solvent molecules.[4] However, fluorescence dynamic Stokes shift measurement can only be applied to a system that has a relatively large reorganization energy for the solvation process.[10] Most of the studies using this method so far focused on the polar solvation dynamics in the electronically excited state.

Recently, photon echo techniques in the electronic transitions have been shown to be a very powerful technique to characterize the magnitudes and the time scales of the dynamical interactions between solute and solvent in room-temperature liquids.[11–16] Traditional two-pulse photon echo measurements have been used to remove the contribution of inhomogeneous broadening from the absorption spectrum; thus, the decay of the signal provides information on the electronic dephasing time (homogeneous broadening).[19] This measurement is very useful when a clear separation for the two line-broadening mechanisms exists in the system. However, the solvation dynamics in room-temperature solution cannot be simply described by the two limiting mechanisms.[12] It has been shown that a three-pulse photon echo experiment, in particular, a photon echo peak shift measurement, is a useful technique to probe such a spectral diffusion process with multiple time scales.[15–17] A peak shift of the photon echo signals was first investigated by Weiner et al.[11] Joo and Albrecht demonstrated the current form of three-pulse photon echo peak shift (3PEPS) measurements.[13] Wiersma and co-workers have performed various types of three-pulse photon echo measurements including the 3PEPS, time-gated photon echo, and heterodyned detected photon echo measurements to study the solvation dynamics of dye molecules in a couple of solvents.[17] Fleming and co-workers performed a series of studies on the solvation dynamics in liquids, glasses, and proteins by using the 3PEPS measurements.[15,16] Furthermore, they have studied the influence of the intramolecular vibration modes in the temporal profiles of the 3PEPS profiles and how the intramolecular vibrational contribution can be separated from the solvation dynamics.[20,21] 3PEPS measurements were also performed for nondipolar solutes in nondipolar solvents to extract the magnitudes and time scales of the solvation dynamics of the nondipolar solute in nondipolar and polar solvents.[22]

In contrast to electronic spectroscopy, vibrational spectroscopy is a very powerful method to study both static and dynamical properties of the molecular structures. Vibrational frequency is very sensitive to the local environments in solution. Extension of the photon echo measurements to the vibrational transitions gives us detailed insights into the solute–solvent interaction and the dynamics of surrounding environments.[23–30] Fayer and co-workers first performed two-pulse vibrational photon echo measurements in the condensed phase by using a free electron laser as an excitation source.[23] They investigated the vibrational dephasing dynamics in low temperature glasses and solutions. Thanks to a rapid development of Ti:Sapphire laser-based technology, ultrafast infrared pulses are routinely produced by tabletop laser systems and are used for the vibrational echo measurements.[24–26] Hamm et al. first used such pulses to perform three-pulse infrared photon echo measurements for the anti-symmetric stretching mode of azide ion in water.[24] Infrared photon echo measurements were also applied for various systems.[25–27] For example, Stenger et al. studied the vibrational dynamics of the OH stretching mode of HOD in D_2O with two-pulse and three-pulse photon echo measurements to investigate the dynamics of the hydrogen-bond network of water.[27] Furthermore, two-dimensional nonlinear infrared spectroscopies, a vibrational analogue of 2D NMR, have become powerful techniques to study the structure and dynamics of the molecular systems and proteins.[28,29] In the 2D photon echo spectra, the existence of cross peaks reflects the couplings and orientations between different vibrational modes; such study is very useful to characterize the conformational dynamics of the molecules on a picosecond time scale. Hochstrasser and co-workers have used heterodyned 2D photon echo measurements to investigate the structures and dynamics of small peptides in solution.[28] Tokmakoff and co-workers have investigated the vibrational correlation of two carbonyl stretching modes of $[Rh(CO)_2C_5H_7O_2]$ by two-dimensional IR spectroscopy.[29] Very recently, Fayer and co-workers have applied this method to investigate the dynamics of hydrogen bonds in methanol oligomers and water (HOD in H_2O).[30]

Recently, we have performed infrared photon echo and transient grating measurements to study the solvation dynamics and vibrational population relaxation processes of small ions, and polyatomic molecules in solutions.[31–36] We have also extended the investigation of the solvation dynamics of azide ion in confined systems such as the reverse micelles.[34a] In this paper, we review our recent works on the dynamical interaction between solute and solvent by nonlinear infrared spectroscopy. We will mainly discuss the results for small ions such as OCN^-, SCN^-, and $[Fe(CN)_6]^{4-}$ in solution.[31–33] The paper is organized as follows. The principles of the three-pulse photon echo method and the theoretical background of nonlinear infrared spectroscopy are described in section **1**. In section **2.1**, we present some studies on solvation dynamics of the vibrational states for triatomic ions such as OCN^- and SCN^- in methanol.[31] In sections **2.2** and **2.3**, we describe the vibrational population relaxation and solvation dynamics of $[Fe(CN)_6]^{4-}$ in D_2O and H_2O.[32,33]

1. Principles

1.1 Characterization of the Dynamical Interaction between Solute and Solvent. The key observable quantity to characterize the solvent fluctuations in the photon echo measurement is the correlation function of the transition frequency fluctuation, $M(t)$.[37]

$$M(t) = \langle \delta\omega(t)\delta\omega(0)\rangle, \tag{1}$$

where $\delta\omega(t)$ is the deviation of the transition frequency at time t from the average value and the brackets indicate the ensemble averaging. The correlation function is related to the loss of the memory of the initial transition frequency, which gives us an idea of the magnitudes and time scales of the dynamical interactions between solute and solvent, as schematically shown in Fig. 1. When we assume very fast modulation of the transition frequency, the form of the correlation function becomes close to a delta function, which means the instantaneous loss

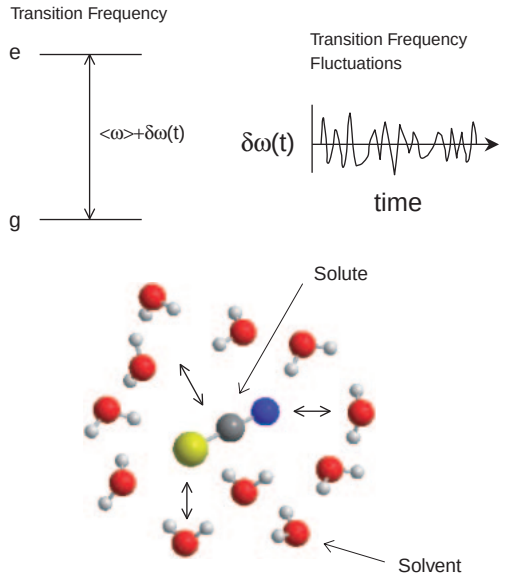

Fig. 1. Schematic representation for transition frequency fluctuations and the correlation function of the transition frequency fluctuations. Transition frequency defines as an energy difference between the ground and excited states. Transition frequency at time t is given by $\langle\omega\rangle + \delta\omega(t)$ where $\langle\omega\rangle$ is the average value and $\delta\omega(t)$ is the deviation from the average value. The value of $\delta\omega(t)$ changes as a function of time due to the solvent fluctuation. The correlation function of the transition frequency fluctuations, $\langle\delta\omega(t)\delta\omega(0)\rangle$, provides information on the magnitudes and time scales of the dynamical interaction between solute and solvent.

of the correlation. This case is the so-called motional narrowing limit and the lineshape of the spectrum is determined by the homogeneous broadening.[8] On the other hand, in the slow modulation limit or when there is static distribution of the frequency due to the inhomogeneity of the system, the correlation function gives a constant value and its lineshape is determined by the inhomogeneous broadening.[8] The real situations in the room-temperature liquids are located in the middle between the two extreme cases. Any solvent fluctuation induces the loss of the memory of the initial solvation environment, which leads to the decay of the correlation functions of the transition frequency fluctuations on various time scales. Therefore, the form of the correlation function provides a measure of the solvation dynamics.

Various third-order nonlinear optical spectroscopies, such as the transient absorption, transient grating, and photon echo techniques, have been used to extract information on the correlation function of the transition frequency fluctuations.[12–17,24–27] The temporal profiles of the peak shifts or the first moments in the three-pulse photon echo signals provide detailed information on the correlation function of the transition frequency fluctuations.[4,15,17,24–26] Cho et al. and de Boeij et al. derived an analytical formula for the temporal profiles of the peak shift in the three-pulse photon echo signals for the impulsive limit.[38] They found that the temporal profiles of the peak shift mirror the correlation function of the transition frequency fluctuations except at the short times.[38] Generally, by including the finite pulse width of the laser pulses, the parameters for the correlation functions can be obtained with a numerical simulation of the photon echo signals.[15–17] On the other hand, transient grating measurements give us complimentary information on the dynamics of the system such as the population relaxation.[39] In the next section, we briefly review the theoretical background for the three-pulse photon echo and transient grating methods.

1.2 Experimental Configuration. The three-pulse photon echo and transient grating methods belong to the family of the four-wave mixing spectroscopies that are based on the third-order optical nonlinear phenomena.[37] An experimental setup for these measurements is shown in Fig. 2. The output of a Ti:Sapphire regenerative amplifier is used to pump an optical parametric amplifier. A tunable femtosecond IR pulse was generated by difference frequency mixing between the signal and the idler of the optical parametric amplifier in a $AgGaS_2$ crystal.[40] For the experiments, the laser beam is split into three and these beams are focused at the sample with an off-axis parabolic reflector in a boxcar geometry. The nonlinear optical signals are measured in the phase-matched directions $-\mathbf{k_1} + \mathbf{k_2} + \mathbf{k_3}$, where $\mathbf{k_1}$, $\mathbf{k_2}$, and $\mathbf{k_3}$ are the wavevectors of the first, second, and third pulses, respectively. The signal was detected by a liquid nitrogen-cooled indium antimonide (InSb) detector and processed by a boxcar-gated integrator and a lock-in amplifier. We used a He–Ne laser for the alignment of the IR pulses. The polarization of the laser pulses was controlled with

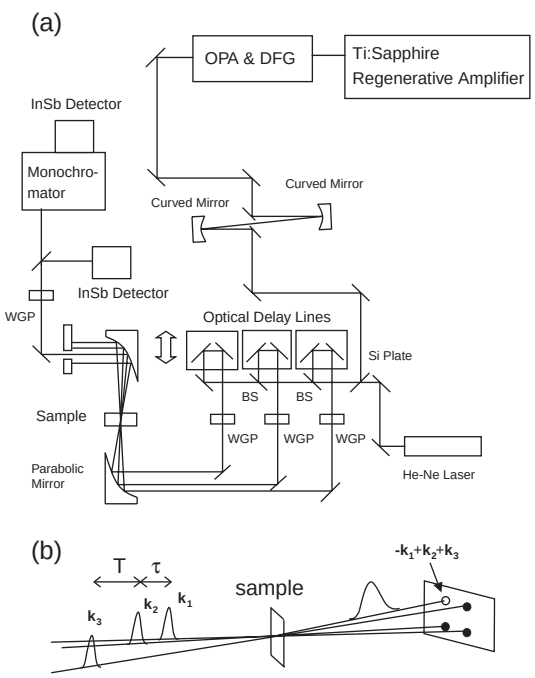

Fig. 2. (a) Schematic diagram of the experimental setup for infrared photon echo and transient grating measurements. Abbreviations are follows: OPA, Optical parametric amplifier; DFG, Difference frequency generator; BS, Beam splitter; WGP, Wire grid polarizer. (b) Experimental configuration for three-pulse photon echo method. Open circles represent the position of the photon echo signals at $-\mathbf{k_1} + \mathbf{k_2} + \mathbf{k_3}$.

wire-grid polarizers. Time delays between two beams are controlled independently by motorized delay lines. Here, τ is defined as time delay between $\mathbf{k_1}$ and $\mathbf{k_2}$ beams, while T is defined as the time delay between $\mathbf{k_2}$ and $\mathbf{k_3}$ beams for $\tau > 0$ or between $\mathbf{k_1}$ and $\mathbf{k_3}$ beams for $\tau < 0$.[15] For the three-pulse photon echo measurements, the signal is recorded by scanning the time delay τ for a fixed time delay T. For the transient grating measurements, τ is set to zero and the signal is measured by scanning the time delay T.

1.3 Theoretical Background. The details of the theory for nonlinear optical spectroscopy including the photon echo and transient grating measurements have been described earlier.[26,37] Here, we briefly review the essential points of the theory. Experimentally observed nonlinear optical signals can be expressed by a time-integrated intensity of the third-order optical polarization, which is given by

$$I(\tau, T) \propto \int_0^\infty |P(t; T, \tau)|^2 \mathrm{d}t, \tag{2}$$

where $P(t; T, \tau)$ is the third-order nonlinear polarization at time t. The third-order polarization is expressed by a convolution of the response function with the electric fields of the laser pulses. The detailed description of the response functions was given elsewhere.[26,37] The response function can be calculated from the line broadening function $g(t)$. The relation between $g(t)$ and $M(t)$ is given below.

1.3.1 Three-Pulse Photon Echo Method: For understanding the principle of the traditional photon echo measurements, a vector model of the optical Bloch equations or an analogy of the foot race is often used.[23,41] Furthermore, Fleming gives an intuitive picture for explaining the principles of the three-pulse photon echo measurements by an analogy to ray optics.[42] Here, we only give a part of theory necessary to understand the essentials of the infrared photon echo measurements. For the intuitive understanding of the photon echo measurements, we just refer to the book and the papers.[23,41,42]

For infrared photon echo measurements, we consider the three vibrational levels for the nonlinear optical signals, since the transition between $\nu = 1$ and $\nu = 2$ states for our system is located within the bandwidth of the infrared pulses. It is assumed that these vibrational states of the solute are linearly coupled with a solvent bath. The solvent bath is generally approximated by a quasicontinuous set of harmonic oscillators, which is referred to as the spin-boson model or the multimode Brownian oscillator model.[4,15,37] Various contributions for the third-order nonlinear optical polarization are expressed by double-sided Feynman diagrams.[37] Each Feynman diagram represents the time evolution of the density operator under the interactions with the laser light. The response function is a sum of contributions from all the Feynman paths. We briefly describe the eight relevant Feynman diagrams for the photon echo signals in the vibrational transitions (Fig. 3).[24,26] When τ is positive, the first three diagrams (R_1, R_2, and R_3) contribute to the photon echo signals. For the diagram R_1, the first laser pulse produces a coherence between the $\nu = 0$ and $\nu = 1$ levels. This coherence is destroyed by the dephasing process, i.e., the fluctuation of the surrounding solvent molecules. After time τ, the second laser pulse transfers the system into the population state. The population state proceeds in the $\nu = 1$ level. The third pulse produces the coherence state again; this is the complex conjugate of the first coherence state. Since the system propagates towards the initial coherence, this contribution gives the rephasing of the macroscopic polarization and hence gives an echo signal. The diagram R_2 is also a rephasing diagram where the system evolves in the $\nu = 0$ level during the time delay T. The diagram R_3 involves the coherence of the $\nu = 1$–2 transition during the time period t. The signal from this contribution is emitted from $\nu = 1$ level. The diagrams R_4, R_5, and R_6 contribute to the signal when τ is negative. These are so-called non-rephasing diagrams which give free induction decays because the second coherence state has the same phase factor (not complex conjugate) as the first one that is also destroyed by the dephasing process. R_7 and R_8 contribute to the signal only when T is close to zero.[26]

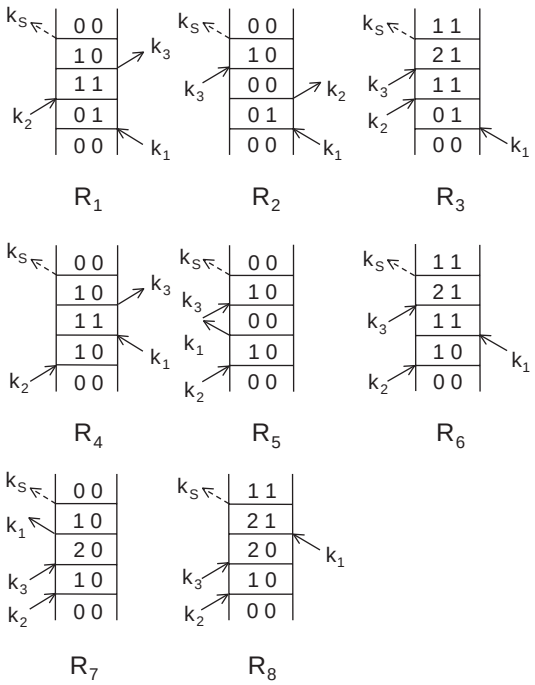

Fig. 3. Double-side Feynman diagrams that contribute to the photon echo signals. "0", "1", and "2" denote the $\nu = 0$, $\nu = 1$, and $\nu = 2$ levels. Time evolution of the density matrix is given by two vertical lines. Left (right) line corresponds to the ket (bra) side of the density matrix. Time proceeds from bottom to top. The interaction of the laser pulse is described by an arrow. The arrow going from left to right is a positive wavevector, while that from right to left is a negative wavevector.

When the system has an inhomogeneous distribution of the transition frequencies, contributions of the rephasing pathways become greater than those of non-rephasing ones. Therefore, the peak of the photon echo signal is located at the positive side of τ when the delay time τ is scanned with a fixed T. As the delay time T increases, dynamical fluctuations of the surrounding solvents destroy the inhomogeneity of the distribution of the transition frequencies. When the imhomogeneity is washed out completely due to the spectral diffusion, rephasing and non-rephasing diagrams contribute equally to the sig-

nals. In this case, the photon echo signal becomes symmetric with respect to $\tau = 0$ fs and the peak of the photon echo signal is located at zero. Therefore, the peak shift or the first moment of the photon echo signals is a sensitive measure for the degree of the "transient" inhomogeneity in the distribution of the transition frequencies.[4,11–17,24–27] Finite peak shifts at long times correspond to the presence of inhomogeneity.

For our system, the temporal profile of the photon echo signal is highly asymmetric with respect to τ at small delay time T, as shown later.[24,31–33] Therefore, we use the first moment of the photon echo signals rather than the peak shift in order to characterize the degree of "transient" inhomogeneity. The first moment is defined as follows:

$$FM(T) = \frac{\int_{-\infty}^{\infty} \tau I(\tau, T) \mathrm{d}\tau}{\int_{-\infty}^{\infty} I(\tau, T) \mathrm{d}\tau}, \quad (3)$$

where $I(\tau, T)$ is the experimental photon echo signal at the delay times τ and T.

The response function can be calculated in terms of the line broadening function. The line broadening function $g(t)$ is given by

$$g(t) = \int_0^t \mathrm{d}t_1 \int_0^{t_1} \mathrm{d}t_2 M(t_2). \quad (4)$$

It should be noted that the Stokes shift is considered to be small for the vibrational transitions.[24] Therefore, the imaginary part of $g(t)$ can be neglected. Here, we assume that the anharmonicity fluctuation is small, so that the vibrational frequency fluctuation of $\nu = 1$–2 transition is the same as that of $\nu = 0$–1 transition. Since the vibrational population relaxation takes place on similar time scales to the vibrational dephasing processes, we included the population kinetics in the response functions. We assume that the population relaxation time from the $\nu = 2$ state is a half of that from the $\nu = 1$ state because the population relaxation time is inversely proportional to the vibrational quantum number in the harmonic approximation.[43]

1.3.2 Transient Grating Method: In parallel with the photon echo measurements, the transient grating or transient absorption measurements should be performed in order to obtain complimentary information on the dynamical processes in solution.[32,33] For transient grating measurements, the first two pulses overlap temporally ($\tau = 0$). These first two pulses create the population state either in the ground state or in the excited state. By scanning the time delay T, one can monitor various dynamical processes, such as the population relaxation, the spectral diffusion (solvation dynamics), and the spatial diffusion (thermal and mass diffusion).[15,39,44] Intuitively, one can easily understand the origin of the signals by considering a formation and destruction of the grating. By the interference of the first two pulses, a sinusoidal modulation of the light intensity is created in the sample. According to this modulation, the grating is formed due to the changes of the refractive index and absorbance of the sample. This grating is monitored by the diffraction of the third pulses. From the decay of the transient grating signals, one can obtain information on the population relaxation, thermal diffusion, and mass diffusion processes.[39]

2. Nonlinear Infrared Spectroscopic Studies for Vibrational Transitions

2.1 Solvation Dynamics of Vibrational Transitions of OCN^- and SCN^- in Methanol. In recent years, an extensive effort has been devoted to investigate the vibrational dynamics of small ions in the condensed phase. Studies on simple diatomic and triatomic ions provide detailed physical base for solute–solvent interactions and serve as a good test for theoretical modeling.[45–49] Based on the results of the steady-state vibrational spectra, the frequencies and the linewidths of the vibrational transitions on these small ions are well characterized both in gas phase and in solutions.[45,50] Furthermore, the dynamical properties, such as the vibrational population relaxation times and the reorientational times, have also been studied by time-resolved vibrational spectroscopy.[46,51] We have used three-pulse IR photon echo method to determine the correlation functions of the vibrational frequency fluctuations of the anti-symmetric stretching modes for OCN^- and SCN^-.[31] The correlation function reflects the magnitudes and time scales of the fluctuations of the solute–solvent interaction, which is monitored by the solvent-induced vibrational frequency perturbations.

Figure 4 shows the three-pulse photon echo signals of OCN^- in methanol at three different delay times T. At $T =$ 300 fs, the peak of the photon echo signals is located at around 300–350 fs. An asymmetric profile of the photon echo signal against the delay time τ was observed. As can be clearly seen in Fig. 4, a finite peak shift of the photon echo signal at $T =$ 300 fs indicates the presence of an inhomogeneous distribution

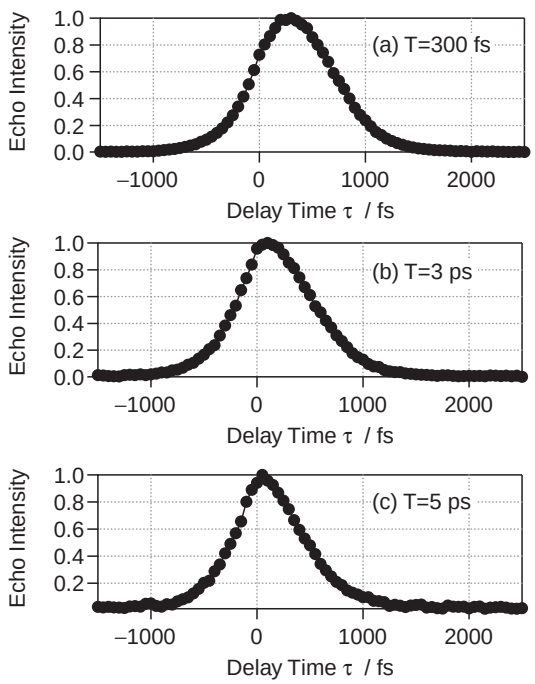

Fig. 4. Three-pulse photon echo signals of OCN^- in methanol at three different delay times T. (a) 300 fs, (b) 3 ps, (c) 5 ps. A mid-IR pulse used for the measurement has a 140–160 fs pulse width and a 120–130 cm^{-1} bandwidth. The center frequency of the laser pulse is 2150 cm^{-1}.

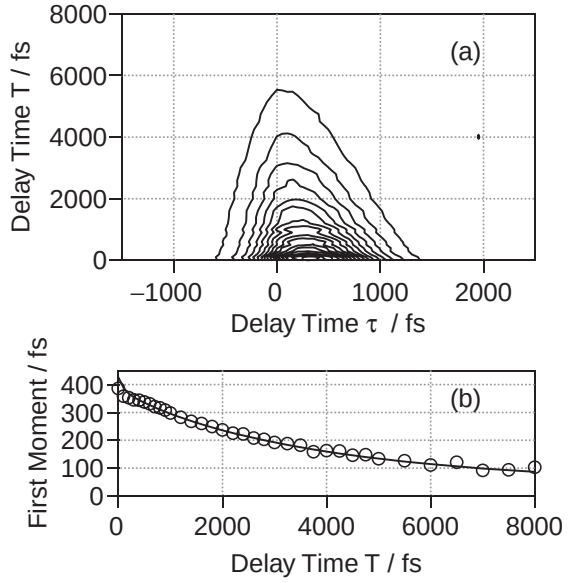

Fig. 5. (a) Three-pulse photon echo signals plotted against the delay times τ and T for OCN^- in methanol. The pulse characteristics are the same as in Fig. 4. (b) The first moment of the photon echo signals from the experimental data (open circles) and from the simulation (solid line).

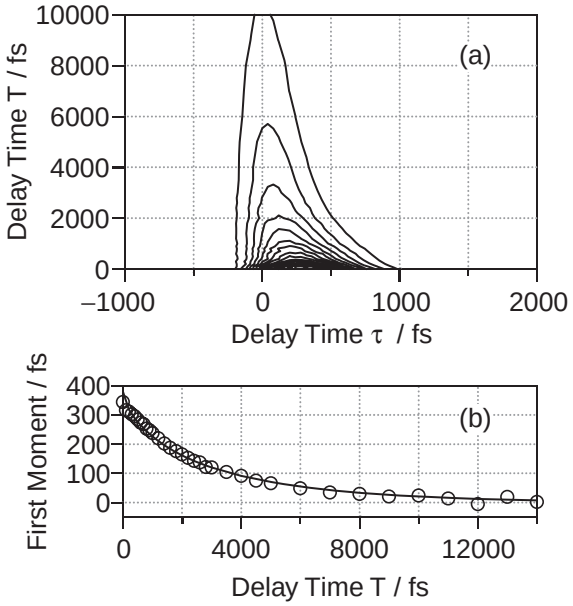

Fig. 6. (a) Three-pulse photon echo signals plotted against the delay times τ and T for SCN^- in methanol. The center frequency of the laser pulse is 2054 cm^{-1}. (b) The first moment of the photon echo signals from the experimental data (open circles) and from the simulation (solid line).

of the vibrational transition frequency. As T increases, the peak of the signal shifts towards zero. Figure 5a displays the three-pulse photon echo signals of OCN^- in methanol plotted as functions of delay times τ and T. The first moments of the echo signals at different delay time T were calculated according to Eq. 3; the results are shown in Fig. 5b. The first moment starts at around 400 fs and decays to 100 fs on a 4 ps time scale. The total intensity of the photon echo signals decreases on a few ps time scale because the vibrational relaxation process for the anti-symmetric stretching mode of OCN^- in methanol takes place on a 3 ps time scale.

The photon echo signals of SCN^- in methanol are plotted in Fig. 6 as a function of the delay times τ and T along with the temporal profile of the first moment of the photon echo signals. Decay of the photon echo signal for SCN^- is faster than that for OCN^- so that the temporal width is narrower for SCN^-, which means that the vibrational dephasing time for SCN^- is faster than that for OCN^-. A faster decay of the photon echo signal for SCN^- reflects a stronger system-bath interaction for SCN^- compared to that for OCN^-. This is consistent with the difference of the width of the absorption spectra observed between OCN^- and SCN^-. For SCN^-, the first moment of the photon echo signal decays to zero on a 4 ps time scale and is close to zero at $T = 14$ ps. This indicates a very small static inhomogeneity at a longer delay time T.

By simulating the temporal profiles of the photon echo signals and comparing them with the experimental results, the parameters for the correlation function of the vibrational frequency fluctuations were determined. The correlation function is expressed by a sum of two exponential functions with a constant term, as follows:

$$M(t) = \langle \delta\omega_{01}(t)\delta\omega_{01}(0)\rangle = \sum_{i=1}^{2} {\Delta_i}^2 \exp(-t/\tau_i) + {\Delta_0}^2. \quad (5)$$

Here, Δ_i and τ_i correspond to the coupling strength to solvent and the time scale of the frequency fluctuation, respectively. The parameters used in the simulation are shown in Table 1. $M(t)$ has two decaying time constants: 90–120 fs and 4.1–4.5 ps. The constant term in $M(t)$ represents a decay component whose time scale is longer than our measurement (~8 ps). A fast decaying component cannot be clearly seen in the temporal profile of the first moment. However, it is necessary to include this component in order to simulate both the absorption spectra and the temporal profile of the photon echo signals with a single set of the parameters. The parameters for the fast decaying component are not well determined. This is because this component falls into the fast modulation limit and only the values of ${\Delta_1}^2\tau_1$ are important to characterize the vibrational dephasing process. It was found that the time constants of the frequency fluctuations for two components are quite similar for SCN^- and OCN^-, while the amplitudes of the fluctuations for SCN^- are about twice as large as those for OCN^-. We also simulated the absorption spectra of the anti-symmetric stretching mode of OCN^- and SCN^-. Good agreement between the experimental results and the simulation is obtained.[31]

In the previous three-pulse IR photon echo studies of N_3^- in D_2O, it was found that the correlation function decays with time constants of 80 fs and 1.3 ps.[24] The time constants of the slowly decaying component for OCN^- and SCN^- in methanol are clearly different from those of N_3^- in D_2O. The amplitude of the vibrational frequency fluctuation for the slowly decaying component in methanol is larger than that in D_2O. Studies on the molecular dynamics simulations for CN^- in water and methanol suggested that the time scale of the making and breaking of the hydrogen bonds in methanol is about three times (for CN^-) slower than that in water.[47] Furthermore,

Table 1. Parameters of the Correlation Function of the Vibrational Frequency Fluctuations, the Vibrational Population Relaxation Times, Rotational Diffusion Constants, and Anharmonicities for OCN^- and SCN^- in Methanol

Solutes	Δ_1/ps^{-1}	τ_1/ps	Δ_2/ps^{-1}	τ_2/ps	Δ_0/ps^{-1}	T_1/ps[a)]	Rotational diffusion constants/ps^{-1} [a)]	Anharmonicity/cm^{-1} [a)]
OCN^-	1.3	0.12	1.6	4.5	0.55	2.9	0.025	28
SCN^-	2.6	0.09	3.6	4.1	0.1	11.0	0.019	23

a) Taken from Ref. 46.

molecular dynamics simulations for N_3^- in methanol showed that the "hydrogen bond" lifetime in methanol is 2.1 ps.[47]

Our results demonstrated that the coupling strength to the solvent is larger for SCN^- than for OCN^-. This observation seems inconsistent with the trends for the vibrational population relaxation and reorientation relaxation processes for both ions. Hochstrasser and co-workers investigated the vibrational population relaxation processes of the anti-symmetric stretching mode for N_3^-, OCN^-, and SCN^- in several protic and aprotic solvents.[46] They suggested that longer vibrational relaxation time and shorter reorientation time for SCN^- are due to weak interactions with solvent compared to those for N_3^- and OCN^-. To address the origin of such a difference, we first consider the pathway for the vibrational population relaxation process. Vibrational population relaxation takes place either as a direct relaxation to the ground state or as an intramolecular vibrational energy redistribution (IVR) to the other modes. Theoretical studies of N_3^- in water by Morita et al. showed that the direct relaxation to the ground state and the IVR to the symmetric stretching mode contribute equally to the overall vibrational population relaxation.[49] They also showed that the charge fluctuation effect of the ion greatly enhances the relaxation rates of both the processes.[49] We can consider that a contribution of IVR process to the overall rate could be different between OCN^- and SCN^-. This would cause different vibrational population relaxation times for the two different ions. Regarding the different behaviors for the vibrational population relaxation and the solvation dynamics, we consider that the IVR process may play an important role in the population relaxation.

As discussed previously, both the vibrational relaxation times and the correlation function of the vibrational frequency fluctuations are related to the correlation function of the linear force which is exerted by the solvent.[7] If the Fourier transform of the correlation functions of the linear force has similar frequency dependence for both ions and if the direct relaxation to the ground state dominates in the overall relaxation, the vibrational population relaxation should be correlated with the vibrational dephasing times. The force acting on a vibrational coordinate depends on the charge distribution and on the form of the normal coordinates of the ions, causing different contributions to the vibrational population relaxation and vibrational dephasing process. Furthermore, the correlation function of a higher order force may contribute to the correlation function of the vibrational frequency fluctuations.[52]

We also would like to address the influence of the solvent-induced frequency shifts, charge distributions and form of the normal coordinates for OCN^- and SCN^-. The frequencies of the anti-symmetric stretching modes for OCN^- and SCN^- in the gas phase are 2124.3 cm^{-1} and 2065.9 cm^{-1}, respectively.[46] The peak frequency is blue-shifted by about 37 cm^{-1} for OCN^- in methanol compared to that in the gas phase, while there is a small shift in SCN^-.[46] These trends correlate with the vibrational relaxation times for these ions, but not with the linewidths of the absorption spectra. The solute–solvent interactions can be classified into repulsive and attractive parts. The frequency shift due to the repulsive part has a different sign from that due to the attractive part.[53] The higher frequency in solution for OCN^- suggests a relatively greater importance of the repulsive part compared to that of the attractive part. Therefore, it is plausible that the total shift becomes smaller for SCN^- because of the cancellation of two contributions with the similar magnitudes even though the magnitude of the shift for each contribution is greater for SCN^- than that for OCN^-. It is quite an interesting problem to investigate the relation between the observed dynamics and the nature of the solvent–solute interaction, namely how the repulsive and attractive parts of the interaction are related with the fast and slow components.

2.2 Vibrational Population Relaxation and Solvation Dynamics of $[Fe(CN)_6]^{4-}$ in D_2O. Since $[Fe(CN)_6]^{4-}$ has O_h symmetry, the IR-active CN stretching modes are triply degenerate.[54] The directions of the anti-symmetric motions of the triply degenerate CN stretching mode (T_{1u} mode) are orthogonal to each other. An anti-symmetric CN stretching motion originates from the opposite in-line CN pairs. For such a system, it is crucial to obtain information on the time evolution of the population distribution process among the three states of the T_{1u} mode, because the population distribution process could affect the vibrational dephasing process. Dynamical interaction between solute and solvent induces symmetry breaking of the triply degenerate mode. This might cause some unique dephasing mechanism which does not exist for the non-degenerate system. In this study, we have used the transient grating measurements to investigate the vibrational population relaxation processes, while the three-pulse photon echo measurements have been used to determine the form of the correlation function of the vibrational frequency fluctuations.[32]

Figure 7 shows the linear IR absorption and Raman spectra of $[Fe(CN)_6]^{4-}$ in D_2O. From FT-IR measurements, the center frequency of the T_{1u} mode was found to be located at 2036 cm^{-1}.[32] In the polarized Raman spectrum, two bands were observed at 2000–2100 cm^{-1} region, while only one of them was observed in the depolarized Raman spectrum. The peaks of the two Raman bands are located at 2057 and 2094 cm^{-1}.[32] Based on the polarization dependence of the Raman spectra, a band at 2057 cm^{-1} is assigned to the E_g mode and a band at 2094 cm^{-1} is assigned to the A_{1g} mode.[54]

Figure 8 displays the results of the transient grating signals of $[Fe(CN)_6]^{4-}$ in D_2O at the parallel, perpendicular, and mag-

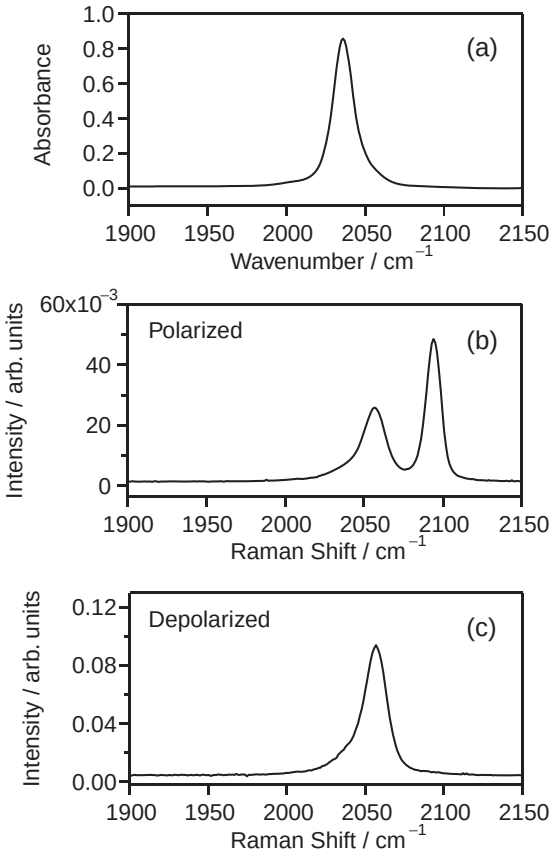

Fig. 7. (a) Linear IR absorption spectrum of the CN stretching mode of $[Fe(CN)_6]^{4-}$ in D_2O. Polarized (b) and depolarized (c) Raman spectrum of the CN stretching mode of $[Fe(CN)_6]^{4-}$ in D_2O.

ic angle polarization conditions of the pump and probe pulses. Due to the homodyne nature of the transient grating signals, we first calculated the square root of the transient grating signals, and then fitted them with a sum of the exponential functions.[39] For the parallel polarization, the transient grating signals decay on two different time scales. On the other hand, for the perpendicular polarization, a slow rising component was observed on a picosecond time scale. On the time scale later than 10 ps, the signals at two different polarization conditions overlap each other. This decays to zero on a 20 ps time scale. For the magic angle conditions, the amplitude of the fast decaying component becomes smaller than that for the parallel polarization condition. The decay time constants of the square root of the magic angle transient grating signals are 0.7 ps and 23.0 ps. The anisotropy of the transient grating signals was calculated from the following equations:[55]

$$r(T) = \frac{\sqrt{I_{\text{parallel}}(T)} - \sqrt{I_{\text{perpendicular}}(T)}}{\sqrt{I_{\text{parallel}}(T)} + 2\sqrt{I_{\text{perpendicular}}(T)}}, \quad (6)$$

where $I_{\text{parallel}}(T)$ and $I_{\text{perpendicular}}(T)$ are the intensity of the transient grating signals on the parallel and perpendicular polarization conditions at the delay time T. The result of the anisotropy decay is shown in Fig. 9. The anisotropy starts at near 0.4 and decays with a time constant of 2.6 ps.

From the decay of the transient grating signals, we can obtain information on the vibrational population relaxation processes. Figure 10 summarizes the population relaxation process of the CN stretching mode of $[Fe(CN)_6]^{4-}$. It is shown that the decay of the transient grating signal within a 5 ps time scale is very sensitive to the polarization of the pump and probe pulses. Anisotropy decay of the transient grating or transient absorption signals is usually assigned to the orientational relaxation of the solute molecule.[2] However, compared with the reorientational times of the other small ions in water, the 2.6 ps decay time is too short for the reorientational dynamics of $[Fe(CN)_6]^{4-}$.

We considered that the anisotropy decay reflects population transfer and/or dephasing among the three states of the T_{1u} mode.[56] The asymmetric stretching modes of the three states are directed along the three axes of the orthogonal coordinate system: x, y, and z. Excitation with the polarized pulse generates superposition states among the three different levels. Fluctuations of the surrounding solvents and/or the coupling with

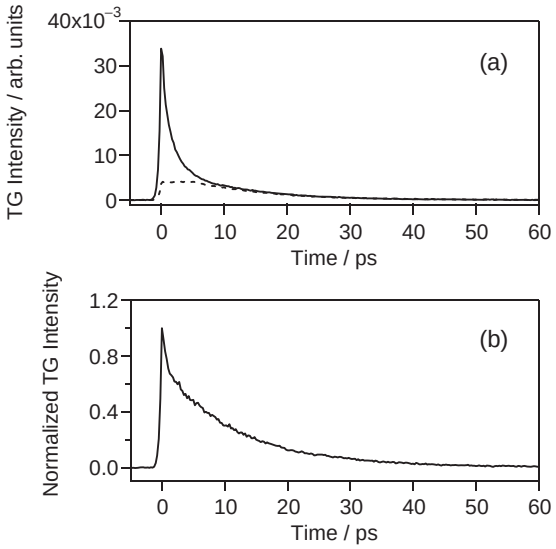

Fig. 8. (a) Transient grating signals of $[Fe(CN)_6]^{4-}$ in D_2O at the parallel (solid line) and perpendicular (dashed line) polarizations. (b) Transient grating signal of $[Fe(CN)_6]^{4-}$ in D_2O at the magic angle condition. A mid-IR pulse used for the measurement has a 140–200 fs pulse width and a 120–130 cm^{-1} bandwidth. The polarization of the laser pulse was controlled by wire-grid polarizers.

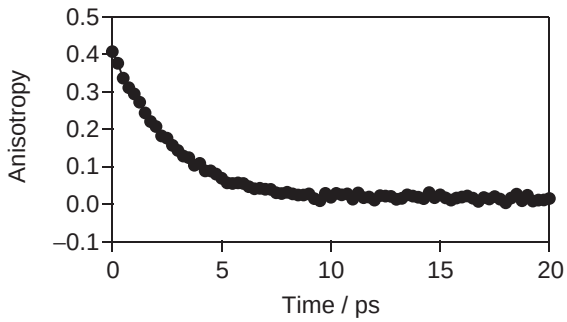

Fig. 9. Anisotropy decay calculated from the experimental data of the transient grating signals at the parallel and perpendicular polarization conditions.

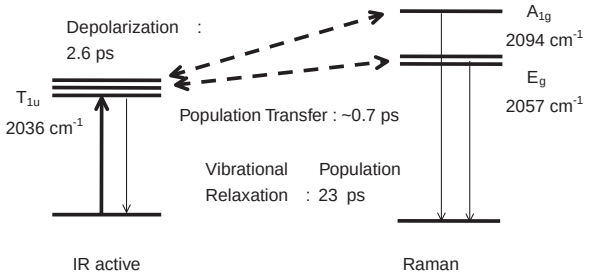

Fig. 10. Summary of the vibration population relaxation process of $[Fe(CN)_6]^{4-}$ in D_2O.

the other intramolecular modes induce the transition from the one state of the T_{1u} mode to the others. Therefore, the direction of the transition dipole moment rotates due to this population distribution among the three different levels. Similar depolarization dynamics were observed in triply degenerate asymmetric CO stretching mode of $W(CO)_6$ in several solvents, which has the same O_h symmetry.[56] Furthermore, Owrutsky and coworkers have very recently investigated both the vibrational population relaxation and the reorientational dynamics of the CN stretching mode for $[Fe(CN)_6]^{4-}$ and $[Fe(CN)_6]^{3-}$ in water and several other solvents by ultrafast infrared pump-probe methods.[57] It was found that the time scales of the anisotropy decay do not depend on the solvent so much, which agree with our results. They also measured the anisotropy decay of both CN and NO stretching modes of pentacyanonitrosylferrate(III) ion $[Fe(CN)_5NO]^{2-}$. For pentacyanonitrosylferrate(III) ion $[Fe(CN)_5NO]^{2-}$, the NO stretching mode is nondegenerate. The anisotropy decay for NO stretching mode was found to be correlated with the solvent viscosity, which can be attributed to the overall molecular rotation.[57] This observation supports our interpretation that the dipole reorientational dynamics are caused by the population distribution among the three vibrational levels.

As shown in Fig. 8, the transient grating signal at the magic angle condition decays with the time constants of 0.7 ps and 23 ps. The fast decaying component of the transient grating signal is due to the population equilibration between the T_{1u} mode and the Raman active E_g and A_{1g} mode.[58] Frequency differences between the T_{1u} mode and the E_g and A_{1g} modes are 21 cm^{-1} and 58 cm^{-1}, respectively. It can be considered that the population transfer to a higher energy level is possible due to the assistance of the low-frequency motions of the solvent. The slow decay component of the magic-angle transient grating signal represents the vibrational population relaxation from the $\nu = 1$ state which takes place on a 23 ps time scale. The obtained time constant for the vibrational population relaxation agrees with the value reported very recently.[57] Owrutsky et al. reported that the vibrational population relaxation times in ethylene glycol and formamide are 27 ps and 43 ps, respectively.[57] The pathway of the population relaxation is a combination of the lower frequency intramolecular modes of the solute molecule and the solvent phonon vibrational modes.

Figure 11 shows the three-pulse photon echo signals of $[Fe(CN)_6]^{4-}$ in D_2O at the parallel polarization condition. At $T = 0$ fs, the peak of the photon echo signal is located at 150–200 fs. The temporal profile of the photon echo signal

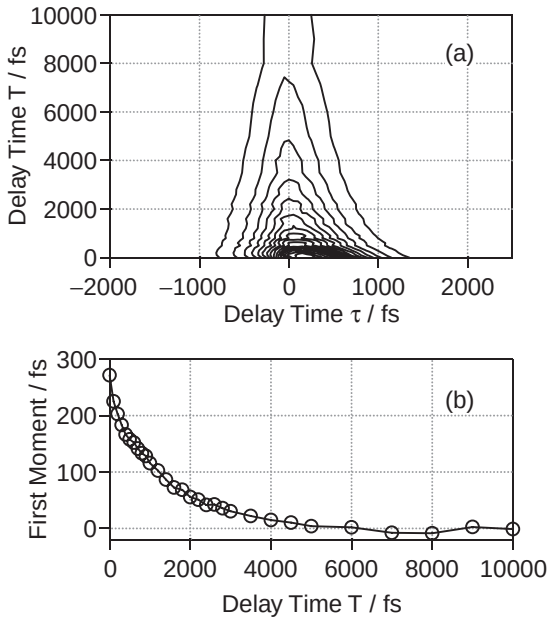

Fig. 11. (a) Three-pulse photon echo signals plotted against the delay times τ and T for $[Fe(CN)_6]^{4-}$ in D_2O. (b) The first moment of the photon echo signals from the experimental data (solid line with open circles).

is asymmetric with respect to τ. The peak of the echo signals shifts towards zero at larger T. The first moments of the photon echo signals were calculated at each delay time T, as shown in Fig. 11b. The first moment decays on a 1.5 ps time scale and is close to zero at $T = 10$ ps. For comparison, we also measured the three-pulse photon echo signals for the anti-symmetric stretching mode of SCN^- in D_2O.[32] Like that of $[Fe(CN)_6]^{4-}$, the first moment of SCN^- decays on a 1.5 ps time scale and is close to zero at $T = 10$ ps. Temporal width of the photon echo signal for SCN^- is narrower than that for $[Fe(CN)_6]^{4-}$, which indicates a stronger system-bath interaction for SCN^-. From comparison of the simulations with the experimentally observed signals for $[Fe(CN)_6]^{4-}$ and SCN^-, the parameters for vibrational frequency fluctuations were determined; these are shown in Table 2. For $[Fe(CN)_6]^{4-}$, $M(t)$ decay with time constants of 80 fs and 1.5 ps. There is no static inhomogeneity in the system. For SCN^- in D_2O, $M(t)$ decays with time constants of 80 fs and 1.3 ps, which is similar to that for $[Fe(CN)_6]^{4-}$ in D_2O, even though the amplitudes of the correlation function are different.

Along with the results of the triatomic ions in methanol, Tables 1 and 2 show the parameters for characterizing the vibrational frequency fluctuations of ions in solution.[31,32] From this table, we can see that the time scales of the decay of the correlation function do not depend on the solute, while the amplitudes of the decaying components depend on both the solute and the solvent. Since the hydrogen bond dynamics is a short-range electrostatic interaction between the ion and solvent, we would expect that a small change in the charge of the solute would affect the time scale of making and breaking of the hydrogen bond. Our results suggested that the hydrogen bonding dynamics between the solute and solvent are not sensitive to the charge distribution of the solute ions. Similar time scales

Table 2. Parameters of the Correlation Function of the Vibrational Frequency Fluctuations, the Vibrational Population Relaxation Times, Rotational Diffusion Constants, and Anharmonicities for $[Fe(CN)_6]^{4-}$, SCN^-, and N_3^- in D_2O

Solutes	Δ_1/ps^{-1}	τ_1/ps	Δ_2/ps^{-1}	τ_2/ps	Δ_0/ps^{-1}
$[Fe(CN)_6]^{4-}$ a)	2.8	0.08	1.15	1.5	0.0
SCN^- a)	4.3	0.08	2.7	1.3	0.0
N_3^- b)	2.6	0.08	1.4	1.3	0.3

Solutes	T_1/ps	Rotational diffusion constants/ps^{-1}	Anharmonicity /cm^{-1}
$[Fe(CN)_6]^{4-}$ a)	0.70 (17%) 23.0 (83%)	0.064 d)	15
SCN^- c)	18.3	0.035	23

a) Taken from Ref. 32. b) Taken from Ref. 24. c) Taken from Ref. 46. d) Rotational diffusion constant for $[Fe(CN)_6]^{4-}$ is calculated from $D = 1/6\tau_{aniso}$ where τ_{aniso} is the time constant of the anisotropy decay of the transient grating signals.

of the decay of the correlation function were observed in the amide I band of trialanine and *N*-methylacetamide in D_2O, even though the nature of the solute molecule and the character of the vibrational mode are different from those for our system.[59] Very recently, the dynamics of hydrogen-networks in water have been investigated by ultrafast infrared spectroscopy.[27,30,60] In these experiments, the fluctuation of the OH stretching frequency is monitored for diluted solution of HOD in D_2O. Stenger et al. have applied two-pulse and three-pulse IR photon echo methods to study the vibrational dephasing and spectral diffusion processes for this system.[27] Fecko et al. used the same 3PEPS measurement with improved time resolution.[60] The correlation function decays with the time constants of 75 fs and 1.2 ps and exhibits a damped oscillation that peaks at 150 fs. The time scale of the slow decaying component is similar to that for our system. Using molecular dynamics simulations, the researchers can relate the OH frequency fluctuations to microscopic dynamics of the hydrogen-bond network.[60] The results suggested that the fluctuation of the OH stretching frequency results from changes in the molecular electric field that acts on the proton. The slower decaying component of the correlation function is due to the collective structural reorganizations including the collective rearrangement of the hydrogen-bond network. Based on these observations, a longer range interaction such as the electrostatic interaction between solute and solvent may be important for the vibrational frequency fluctuation in the present case, particularly for the slow decaying component of the correlation function of the frequency fluctuation. It is very interesting to know how the hydrogen-bond dynamics between the solute and solvent are correlated with the longer-range interaction to reveal the origin of independence of the vibrational frequency fluctuations on the solute mode.

We would also like to comment on the similarity of the degenerate and non-degenerate systems in terms of the decay of the correlation functions. The decay time constants of the correlation function for $[Fe(CN)_6]^{4-}$ in D_2O are similar to those for N_3^- and SCN^- in D_2O. For the triply degenerate system, the vibrational dephasing could be caused by both the energy gap fluctuation between the $\nu = 0$ and $\nu = 1$ states for the T_{1u} mode and the fluctuation of the energy splitting among the triply degenerate T_{1u} modes. Our result suggested that the time scale of the spectral diffusion process for $[Fe(CN)_6]^{4-}$ is controlled by the same mechanism as that for SCN^-, not by the time-dependent anisotropic solute–solvent interaction.

2.3 Vibrational Dynamics of $[Fe(CN)_6]^{4-}$ in H_2O: Deuterium Isotope Effect of Solvents. We have also investigated the vibrational dynamics of the asymmetric CN stretching mode of $[Fe(CN)_6]^{4-}$ in H_2O to study the deuterium isotope effect of the solvent on the solvation dynamics.[33] A detailed investigation of isotope effect of solvents will provide information on the microscopic origin of the vibrational population relaxation and solvation dynamics. Before describing the vibrational dynamics of $[Fe(CN)_6]^{4-}$ in H_2O, we briefly mention the FT-IR spectrum of $[Fe(CN)_6]^{4-}$ in H_2O. The peak of the absorption spectrum for the asymmetric CN stretching mode is located at 2037 cm^{-1} in H_2O, which is almost same as that in D_2O. The linewidth of the absorption spectrum is also the same as that in D_2O ($\sim$16 cm^{-1}).[33]

Figure 12 shows the transient grating signals at the parallel, perpendicular, and magic angle polarization conditions. From the transient grating measurements, we found that the time constant (3.7 ps) of the slow decaying component of the transient grating signal in H_2O is about six times smaller than that in D_2O (23 ps), while the time scale of the anisotropy decay is similar in the two cases.[32,33] Similar values were also reported very recently by Sando et al.[57] This result shows that the vibrational population relaxation in H_2O takes place significantly faster than that in D_2O. A similar acceleration of the vibrational population relaxation was observed for the other solute molecules. Hamm et al. investigated the vibrational relaxation process of CN^- in water.[61] The vibrational relaxation takes place with the time constants of 71 ps in D_2O and 28 ps in H_2O, respectively. They found a correlation between the vibrational relaxation times of the solute and the IR absorption cross section of the solvent, which would suggest the importance of the coupling to internal solvent modes. For the polyatomic cases, it was reported that the vibrational relaxation times of N_3^- are 2.4 ps in D_2O and 0.81 ps in H_2O.[46,51] A combination band of the bending and the librational mode of the solvent is located at 2125 cm^{-1} in H_2O. Energy flow occurs very efficiently from the solute vibrational mode to this combination

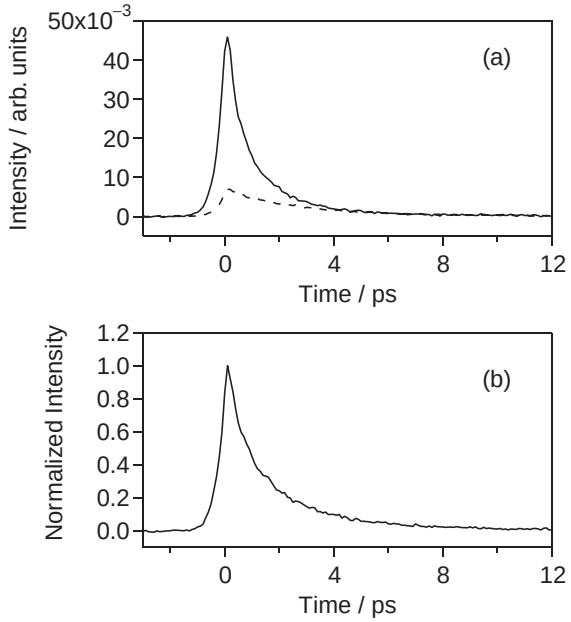

Fig. 12. (a) Transient grating signals of $[Fe(CN)_6]^{4-}$ in H_2O at the parallel (solid line) and perpendicular (dashed line) polarizations. (b) Transient grating signal of $[Fe(CN)_6]^{4-}$ in H_2O at the magic angle condition.

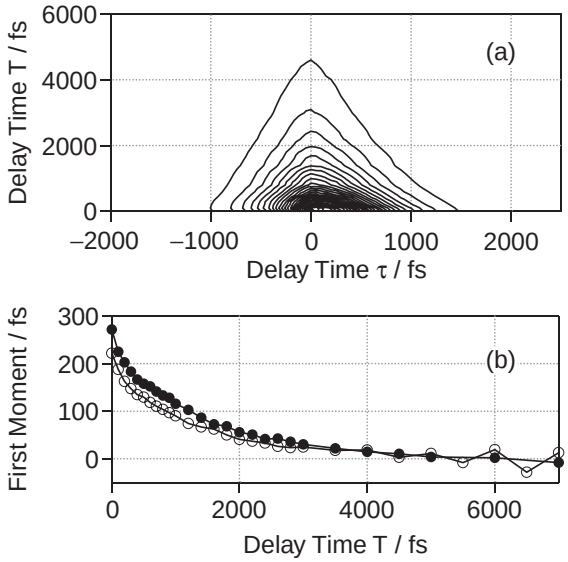

Fig. 13. (a) Three-pulse photon echo signals plotted against the delay times τ and T for $[Fe(CN)_6]^{4-}$ in H_2O. (b) The first moment of the photon echo signals from the experimental data (solid line with open circles). The filled circles represent the first moment of the photon echo signals in D_2O.

band. However, the frequency of the combination band is shifted lower to 1550 cm^{-1} in D_2O so that the energy transfer from the solute to the solvent becomes less efficient in D_2O. We have observed a larger isotope effect on the vibrational population times compared to the other systems. This observation suggests that the intramolecular vibrational energy redistribution is affected by the isotope substitution as well as by the intermolecular energy relaxation.

Figure 13a shows the three-pulse photon echo signals of $[Fe(CN)_6]^{4-}$ in H_2O at the parallel polarization condition. The peak of the photon echo signal is initially located at around 100 fs and shifts towards zero at a longer population time. Figure 13b shows the temporal profiles of the first moments of the photon echo signals in H_2O together with those in D_2O. We found that the time scale of the decay of the first moment is similar for the two cases, even though the magnitude of the first moment in H_2O is slightly smaller than that in D_2O. We simulated the temporal profiles of the photon echo signals based on the correlation function of the vibrational frequency fluctuations. The time scale of the decay of the correlation function in H_2O is very similar to that in D_2O. Very recently, we have also found that the time scale of the decay of the correlation function of the anti-symmetric stretching mode of N_3^- in H_2O is very similar to that in D_2O.[34,35]

For the studies of the solvation dynamics in the electronic transitions, there are some reports on the solvation dynamics in H_2O and D_2O.[62–65] It was shown that the solvation dynamics in D_2O were about 30% slower than in H_2O. These observations were consistent with the results of the theoretical studies based on the molecular hydrodynamic model.[65] On the other hand, we have not observed a noticeable isotope effect for the vibrational solvation dynamics. This indicates that the water molecules respond to a change of the vibrational state in a different manner from the way they respond to the charge redistribution upon the electronic excitation.

3. Conclusion

In this review, we present the results of our recent nonlinear optical spectroscopic studies to investigate the dynamical interaction between solute and solvent in the condensed phase. By monitoring the transition frequency fluctuations in the vibrational states, we can characterize the solute–solvent interactions and solvent dynamics on a wide time scale, from femtoseconds to picoseconds. In particular, the three-pulse photon echo method is very useful technique to extract the form of the correlation function of the transition frequency fluctuations. For vibrational transitions, we have studied the vibrational dynamics of small ions, such as OCN^-, SCN^-, and $[Fe(CN)_6]^{4-}$ in solution by using infrared three-pulse photon echo and transient grating methods. Transient grating measurements were used to determine the time scales of the vibrational population relaxation process. From our results of the three-pulse photon echo measurements, the time scales of the solvation dynamics are mostly determined by the solvent, not by the nature of the vibrational modes of the solute, even though the coupling strength to the solvent depends on the systems we investigated.

Studies on the dynamical interaction between solute and solvent for the vibrational transitions have important implications for understanding the microscopic picture of the solvent fluctuations. Fluctuations of transition frequency include the contribution from both the dynamics of short-range and long-range interactions between the solute and the surrounding solvents. From the studies for the electronic and vibrational transitions, solvation dynamics exhibit bimodal behavior whose time constants range from a ~100 fs to a few picosec-

onds. Similar time scales of the solvation dynamics observed in electronic and vibrational transitions may indicate a correlation of the solvent dynamics between different transitions, even though magnitudes of the transition frequency fluctuations in the electronic and vibrational transitions are very different from each other. In order to answer this question, further studies are necessary, such as probing the electronic and vibrational frequency fluctuations for the same solute molecules. Combination of the studies of theoretical calculations with the experimental ones will give us more detailed information on the nature of the solute–solvent interactions.

We thank Dr. Hiroaki Maekawa for his contribution to this work and Prof. Yasuhisa Mizutani for help with the measurements of steady-state Raman spectrum and for valuable discussions. We also acknowledge Prof. Shinji Saito for valuable discussions. This work was partly supported by a Grant-in-Aid (Nos. 12304036 and 13554019) from the Ministry of Education, Culture, Sports, Science and Technology, and a JSPS research grant for the Future Program. K. O. was supported by a fellowship for Young Scientists from the Japan Society for the Promotion of Science.

References

1 G. R. Fleming and P. Hanggi, "Activated Barrier Crossing," World Scientific, Singapore (1993).

2 G. R. Fleming, "Chemical Applications of Ultrafast Spectroscopy," Oxford University Press, New York (1986).

3 "Ultrashort Laser Pulses and Applications," 2nd ed, ed by W. Kaiser, Springer-Verlag, New York (1993).

4 a) G. R. Fleming and M. Cho, *Annu. Rev. Phys. Chem.*, **47**, 109 (1996). b) W. P. de Boeij, M. S. Pshenichnikov, and D. A. Wiersma, *Annu. Rev. Phys. Chem.*, **47**, 109 (1996).

5 R. M. Stratt and M. Maroncelli, *J. Phys. Chem.*, **100**, 12981 (1996).

6 a) R. G. Gordon, *J. Chem. Phys.*, **43**, 1307 (1965). b) W. G. Rothschild, "Dynamics of Molecular Liquids," Wiley, New York (1984).

7 a) D. W. Oxtoby, *Annu. Rev. Phys. Chem.*, **32**, 77 (1981). b) D. W. Oxtoby, *Adv. Chem. Phys.*, **40**, 1 (1979).

8 a) R. Kubo, "Fluctuation, Relaxation, and Resonance in Magnetic Systems," ed by D. Ter-Haar, Oliver and Boyd, Edinburgh (1962). b) R. Kubo, *Adv. Chem. Phys.*, **15**, 101 (1969).

9 "Ultrafast Dynamics of Chemical Systems," ed by J. D. Simon, Kluwer Academic Publishers, Dordrecht (1994).

10 a) P. F. Barbara and W. Jarzeba, *Adv. Photochem.*, **15**, 1 (1990). b) M. Maroncelli, *J. Mol. Liq.*, **57**, 1 (1993). c) M. L. Horng, J. Gardecki, A. Papazyan, and M. Maroncelli, *J. Phys. Chem.*, **99**, 17311 (1995).

11 A. M. Weiner, S. De Silvestri, and E. P. Ippen, *J. Opt. Soc. Am. B*, **2**, 654 (1985).

12 a) E. T. J. Nibbering, D. A. Wiersma, and K. Duppen, *Phys. Rev. Lett.*, **66**, 2464 (1991). b) E. T. J. Nibbering, D. A. Wiersma, and K. Duppen, *Chem. Phys.*, **183**, 167 (1994).

13 T. Joo and A. C. Albrecht, *Chem. Phys.*, **176**, 233 (1994).

14 a) P. Vöhringer, D. C. Arnett, R. A. Westervelt, M. J. Feldstein, and N. F. Scherer, *J. Chem. Phys.*, **102**, 4027 (1995). b) T.-S. Yang, P. Vöhringer, D. C. Arnett, and N. F. Scherer, *J. Chem. Phys.*, **103**, 8346 (1995).

15 T. Joo, Y. Jia, J.-Y. Yu, M. J. Lang, and G. R. Fleming, *J. Chem. Phys.*, **104**, 6089 (1996).

16 a) S. A. Passino, Y. Nagasawa, T. Joo, and G. R. Fleming, *J. Phys. Chem. A*, **101**, 725 (1997). b) Y. Nagasawa, S. A. Passino, T. Joo, and G. R. Fleming, *J. Chem. Phys.*, **106**, 4840 (1997). c) J.-Y. Yu, Y. Nagasawa, R. van Grondelle, and G. R. Fleming, *Chem. Phys. Lett.*, **280**, 404 (1997). d) T. Joo, Y. Jia, J.-Y. Yu, D. M. Jonas, and G. R. Fleming, *J. Phys. Chem.*, **100**, 2399 (1996). e) Y. Nagasawa, J.-Y. Yu, and G. R. Fleming, *J. Chem. Phys.*, **109**, 6175 (1998). f) R. Jimenez, F. van Mourik, J.-Y. Yu, and G. R. Fleming, *J. Phys. Chem. B*, **101**, 7350 (1997).

17 a) W. P. de Boeij, M. S. Pshenichnikov, and D. A. Wiersma, *Chem. Phys. Lett.*, **238**, 1 (1995). b) W. P. de Boeij, M. S. Pshenichnikov, and D. A. Wiersma, *J. Phys. Chem.*, **100**, 11806 (1996). c) W. P. de Boeij, M. S. Pshenichnikov, and D. A. Wiersma, *J. Chem. Phys.*, **105**, 2953 (1996).

18 a) M. Maroncelli and G. R. Fleming, *J. Chem. Phys.*, **89**, 5044 (1988). b) E. A. Carter and J. T. Hynes, *J. Chem. Phys.*, **94**, 5961 (1991). c) B. M. Ladanyi and M. S. Skaf, *Annu. Rev. Phys. Chem.*, **44**, 335 (1993). d) B. Baguchi and A. Chandra, *Adv. Chem. Phys.*, **80**, 1 (1991). e) F. O. Raneri, H. Resat, B. C. Perng, F. Hirata, and H. L. Friedman, *J. Chem. Phys.*, **100**, 1477 (1994).

19 a) N. A. Kurnit, I. D. Abella, and S. R. Hartmann, *Phys. Rev. Lett.*, **13**, 567 (1964). b) I. D. Abella, N. A. Kurnit, and S. R. Hartmann, *Phys. Rev. Lett.*, **14**, 391 (1965).

20 D. S. Larsen, K. Ohta, Q.-H. Xu, M. Cyrier, and G. R. Fleming, *J. Chem. Phys.*, **114**, 8008 (2001).

21 K. Ohta, D. S. Larsen, M. Yang, and G. R. Fleming, *J. Chem. Phys.*, **114**, 8020 (2001).

22 D. S. Larsen, K. Ohta, and G. R. Fleming, *J. Chem. Phys.*, **111**, 8970 (1999).

23 a) A. Tokmakoff and M. D. Fayer, *Acc. Chem. Res.*, **28**, 437 (1995). b) M. D. Fayer, *Annu. Rev. Phys. Chem.*, **52**, 315 (2001). c) K. D. Rector and M. D. Fayer, "Ultrafast Infrared and Raman Spectroscopy," ed by M. D. Fayer, Marcel Dekker, New York (2000).

24 P. Hamm, M. Lim, and R. M. Hochstrasser, *Phys. Rev. Lett.*, **81**, 5326 (1998).

25 a) M. Lim, P. Hamm, and R. M. Hochstrasser, *Proc. Natl. Acad. Sci. U.S.A.*, **95**, 15315 (1998). b) P. Hamm, M. Lim, and R. M. Hochstrasser, *J. Phys. Chem. A*, **103**, 10049 (1999).

26 P. Hamm and R. M. Hochstrasser, "Ultrafast Infrared and Raman Spectroscopy," ed by M. D. Fayer, Marcel Dekker, New York (2000).

27 a) J. Stenger, D. Madsen, P. Hamm, E. T. J. Nibbering, and T. Elsaesser, *Phys. Rev. Lett.*, **87**, 027401 (2001). b) J. Stenger, D. Madsen, P. Hamm, E. T. J. Nibbering, and T. Elsaesser, *J. Phys. Chem. A*, **106**, 2341 (2002).

28 a) M. C. Asplund, M. T. Zanni, and R. M. Hochstrasser, *Proc. Natl. Acad. Sci. U.S.A.*, **97**, 8219 (2000). b) M. T. Zanni, S. Gnanakaran, J. Stenger, and R. M. Hochstrasser, *J. Phys. Chem. B*, **105**, 6520 (2001). c) M. T. Zanni and R. M. Hochstrasser, *Curr. Opin. Struct. Biol.*, **11**, 516 (2001). d) N. H. Ge and R. M. Hochstrasser, *Phys. Chem. Commun.*, **3**, 1 (2002).

29 a) O. Golonzka, M. Khalil, N. Demirdoven, and A. Tokmakoff, *J. Chem. Phys.*, **115**, 10814 (2001). b) M. Khalil, N. Demirdoven, and A. Tokmakoff, *J. Phys. Chem. A*, **107**, 5258 (2003). c) M. Khalil, N. Demirdoven, and A. Tokmakoff, *J. Chem. Phys.*, **121**, 362 (2004).

30 a) J. B. Asbury, T. Steinel, C. Stromberg, K. J. Gaffney, I. R. Piletic, A. Goun, and M. D. Fayer, *Phys. Rev. Lett.*, **91**, 237402 (2003). b) J. B. Asbury, T. Steinel, C. Stromberg, K. J.

Gaffney, I. R. Piletic, and M. D. Fayer, *J. Chem. Phys.*, **119**, 12981 (2003). c) J. B. Asbury, T. Steinel, C. Stromberg, S. A. Corcelli, C. P. Lawrence, J. L. Skinner, and M. D. Fayer, *J. Phys. Chem. A*, **108**, 1107 (2004). d) T. Steinel, J. B. Asbury, S. A. Corcelli, C. P. Lawrence, J. L. Skinner, and M. D. Fayer, *Chem. Phys. Lett.*, **386**, 295 (2004).

31 K. Ohta, H. Maekawa, S. Saito, and K. Tominaga, *J. Phys. Chem. A*, **107**, 5643 (2003).

32 K. Ohta, H. Maekawa, and K. Tominaga, *J. Phys. Chem. A*, **108**, 1333 (2004).

33 K. Ohta, H. Maekawa, and K. Tominaga, *Chem. Phys. Lett.*, **386**, 32 (2004).

34 a) H. Maekawa, K. Ohta, and K. Tominaga, *Phys. Chem. Chem. Phys.*, **6**, 4074 (2004). b) H. Maekawa, K. Ohta, and K. Tominaga, "MRS Symposium Proceedings" (2004), Vol. 790, p. 6.7.1–p. 6.7.11.

35 H. Maekawa, K. Ohta, and K. Tominaga, *Res. Chem. Intermed.*, in press (2005).

36 a) H. Maekawa, K. Ohta, and K. Tominaga, *J. Phys. Chem. A*, **108**, 9484 (2004). b) H. Maekawa, K. Ohta, and K. Tominaga, *J. Mol. Struct.*, **735–736**, 135 (2005).

37 S. Mukamel, "Principles of Nonlinear Optical Spectroscopy," Oxford University Press, New York (1995).

38 a) M. Cho, J.-Y. Yu, T. Joo, Y. Nagasawa, S. A. Passino, and G. R. Fleming, *J. Phys. Chem.*, **100**, 11944 (1996). b) W. P. de Boeij, M. S. Pshenichnikov, and D. A. Wiersma, *Chem. Phys. Lett.*, **253**, 53 (1996).

39 a) M. D. Fayer, *Ann. Rev. Phys. Chem.*, **33**, 63 (1982). b) H. J. Eichler, P. Gunter, and D. W. Pohl, "Laser Induced Dynamic Gratings," Springer-Verlag, Berlin (1986). c) M. Terazima, *Acc. Chem. Res.*, **33**, 687 (2000).

40 H. Maekawa, K. Tominaga, and D. Podenas, *Jpn. J. Appl. Phys.*, **41**, L329 (2002).

41 a) L. Allen and J. H. Eberly, "Optical Resonance and Two Level Atoms," Dover Publications, New York (1987). b) E. L. Hahn, *Phys. Today*, **6**, 4 (1959). c) R. G. Brewer and E. L. Hahn, *Sci. Am.*, **251**, 50 (1984).

42 G. R. Fleming, *Proc. Natl. Acad. Sci. U.S.A.*, **95**, 15161 (1998).

43 J. T. Fourkas, H. Kawashima, and K. A. Nelson, *J. Chem. Phys.*, **103**, 4393 (1995).

44 K. Ohta, M. Terazima, and N. Hirota, *Bull. Chem. Soc. Jpn.*, **68**, 2809 (1995).

45 a) V. Schettino and I. C. Hisatsune, *J. Chem. Phys.*, **52**, 9 (1970). b) L. H. Jones, *J. Chem. Phys.*, **25**, 1069 (1956).

46 a) J. C. Owrutsky, Y. R. Kim, M. Li, M. Sarisky, and R. M. Hochstrasser, *Chem. Phys. Lett.*, **184**, 368 (1991). b) M. Li, J. C. Owrutsky, M. Sarisky, J. P. Culver, A. Yodh, and R. M. Hochstrasser, *J. Chem. Phys.*, **98**, 5499 (1993). c) J. C. Owrutsky, D. Raftery, and R. M. Hochstrasser, *Annu. Rev. Phys. Chem.*, **45**, 519 (1995).

47 a) M. Ferrario, M. L. Klein, and I. R. MacDonald, *Chem. Phys. Lett.*, **213**, 537 (1993). b) M. Ferrario, I. R. McDonald, and M. C. R. Symons, *Mol. Phys.*, **77**, 617 (1992).

48 R. Rey and J. T. Hynes, *J. Chem. Phys.*, **108**, 142 (1998).

49 A. Morita and S. Kato, *J. Chem. Phys.*, **109**, 5511 (1998).

50 a) M. Polak, M. Gruebele, and R. J. Saykally, *J. Am. Chem. Soc.*, **109**, 2884 (1987). b) M. Gruebele, M. Polak, and R. J. Saykally, *J. Chem. Phys.*, **86**, 6631 (1987). c) M. Polak, M. Gruebele, and R. J. Saykally, *J. Chem. Phys.*, **87**, 3352 (1987).

51 a) Q. Zhong, A. P. Baronavski, and J. C. Owrutsky, *J. Chem. Phys.*, **118**, 7074 (2003). b) Q. Zhong, A. P. Baronavski, and J. C. Owrutsky, *J. Chem. Phys.*, **119**, 9171 (2003).

52 D. W. Oxtoby, D. Levesque, and J.-J. Weis, *J. Chem. Phys.*, **68**, 5528 (1978).

53 A. B. Myers and F. Markel, *Chem. Phys.*, **149**, 21 (1990).

54 a) L. H. Jones, *Inorg. Chem.*, **2**, 777 (1963). b) W. P. Griffith and G. T. Turner, *J. Chem. Soc.*, **1970**, 858.

55 a) R. S. Moog, M. D. Ediger, S. G. Boxer, and M. D. Fayer, *J. Phys. Chem.*, **86**, 4694 (1982). b) A. B. Myers and R. M. Hochstrasser, *IEEE J. Quatum Electron.*, **QE-22**, 1482 (1986). c) E. Vauthey, *Chem. Phys. Lett.*, **216**, 530 (1993).

56 a) A. Tokmakoff, R. S. Urdahl, D. Zimdars, R. S. Francis, A. S. Kwok, and M. D. Fayer, *J. Chem. Phys.*, **102**, 3919 (1995). b) A. Tokmakoff and M. D. Fayer, *J. Chem. Phys.*, **103**, 2810 (1995). c) K. D. Rector and M. D. Fayer, *J. Chem. Phys.*, **108**, 1794 (1998).

57 G. M. Sando, Q. Zhong, and J. C. Owrutsky, *J. Chem. Phys.*, **121**, 2158 (2004).

58 A. Tokmakoff, B. Sauter, A. S. Kwok, and M. D. Fayer, *Chem. Phys. Lett.*, **221**, 412 (1994).

59 S. Woutersen , R. Pfister, P. Hamm, Y. G. Mu, D. S. Kosov, and G. Stock, *J. Chem. Phys.*, **117**, 6833 (2002).

60 C. J. Fecko, J. D. Eaves, J. J. Loparo, A. Tokmakoff, and P. L. Geissler, *Science*, **301**, 1698 (2003).

61 P. Hamm, M. Lim, and R. M. Hochstrasser, *J. Chem. Phys.*, **107**, 10523 (1997).

62 R. Jimenez, G. R. Fleming, P. V. Kumar, and M. Maroncelli, *Nature*, **369**, 471 (1994).

63 P. F. Barbara, G. C. Walker, T. J. Kang, and W. Jarzeba, *Proc. SPIE*, **1209**, 18 (1990).

64 D. Pant and N. E. Levinger, *J. Phys. Chem. B*, **103**, 7846 (1995).

65 N. Nandi, S. Roy, and B. Bagchi, *J. Chem. Phys.*, **102**, 1390 (1995).

Award recipient

Kaoru Ohta was born in Osaka, Japan, in 1969. He graduated from Kyoto University in 1993. He obtained his M.Sci. and Ph.D. degrees in 1995 and 1998, respectively, from Kyoto University under the supervision of Prof. Noboru Hirota. From 1995 to 1998, he was a visiting junior fellow under the supervision of Prof. Keitaro Yoshihara at Institute for Molecular Science. After that, he spent three years at University of California, Berkeley, as a postdoctoral fellow in Prof. Graham R. Fleming's laboratory. In 2001, he became a postdoctoral fellow in Prof. Keisuke Tominaga's laboratory in Kobe University. In 2004, he was a researcher of CREST, JST. Currently, he is a research associate in the Graduate School of Science and Technology, Kobe University. His research interests include the studies of chemical reaction dynamics, relaxation processes, and solvation dynamics in the condensed phase by ultrafast spectroscopy.

Keisuke Tominaga obtained his Ph.D. in 1990 from Kyoto University under the supervision of Prof. Noboru Hirota. After working with Prof. Paul F. Barbara at University of Minnesota as a postdoctoral fellow, he joined the Prof. Keitaro Yoshihara's group of Institute for Molecular Science as a research associate in 1992. In 1998, he moved to Kobe University as an associate professor, and now he is a professor of Molecular Photoscience Research Center of Kobe University. His research interest includes liquid dynamics and reaction dynamics in condensed phases studied by ultrafast laser spectroscopy.